Unifying quasars with clumpy wind models

J. H. Matthews[1,1], C. Knigge[1], N. Higginbottom[1], K. S. Long[2], S. A. Sim[3] and S. W. Mangham[1]

[1]School of Physics and Astronomy, University of Southampton, Highfield, Southampton, SO17 1BJ, United Kingdom
[2]Space Telescope Science Institute, 3700 San Martin Drive, Baltimore, MD, 21218
[3]School of Mathematics and Physics, Queens University Belfast, University Road, Belfast, BT7 1NN, Northern Ireland, UK

August 27, 2015

ABSTRACT

Various unification schemes for quasars and luminous active galactic nuclei (AGN) propose that much of their complex phenomenology can be explained by a simple geometrical picture involving an accretion disc and associated outflow. Here, we test this paradigm by utilising our state-of-the-art radiative transfer and photoionization code to produce synthetic spectra from simple biconical disc wind models. In particular, we expand on our previous work by presenting a model that exhibits many of the spectral features expected from a quasar unification model. We find that a simple treatment of clumping ('microclumping') allows for a more realistic X-ray luminosity in the model, while maintaining the ionization state necessary for strong BAL features. We examine the X-ray properties of this new model and find good agreement with existing X-ray samples of AGN and quasars. We find that the dense, X-ray heated wind produces strong recombination and collisionally excited line emission in, e.g., C IV and Ly α, to emerge at the low inclination, 'Type 1 quasar-like' angles. The highest inclination models possess prominent Mg II and Al III BALs, the absorption features seen in LoBAL quasars. Despite these successes, we are unable to reproduce the remarkably uniform emission line properties seen in BAL and non-BAL quasar composites. This is due to a fundamental constraint arising from the anisotropy of emission from a classical thin disc. We briefly explore the impact of general relativistic effects on the angular distribution of disc continuum emission, and find that they are not sufficient to produce a self-consistent model. Overall, our work suggests that geometric unification involving an accretion disc wind is a promising scenario, but our results pose a number of difficult challenges to such a model.

[1]jm8g08@soton.ac.uk

1. Introduction

The spectra of quasars and luminous active galactic nuclei (AGN) typically exhibit a series of strong emission lines with an underlying blue continuum - the so-called *'big blue bump'* (BBB). The BBB is often attributed to emssion from a geometrically thin, optically thick accretion disc surrounding the central black hole, similar to that described by Shakura & Sunyaev (1973). In addition to the inflowing accreting material, i outflows are ubiquitous in AGN and quasars (Kellermann et al. 1989; Ganguly & Brotherton 2008). These outflows can take the form of highly collimated radio jets (e.g. Hazard et al. 1963; Potash & Wardle 1980; Perley et al. 1984; Marscher 2006), or mass-loaded 'winds' emanating from the accretion disc (Weymann et al. 1991; Turner & Miller 2009). Outflows in AGN offer a potential feedback mechanism through which the central source can affect its environment (King 2003, 2005; Fabian 2012) – feedback that is required in models of galaxy evolution (Springel et al. 2005) and may explain the '$M - \sigma$' relation (Silk & Rees 1998; Häring & Rix 2004).

Approximately 20% of quasars exhibit blueshifted ($\sim 0.1c$) broad absorption lines (BALs) in the ultraviolet, providing clear evidence for outflowing absorbing material (Weymann et al. 1991; Reichard et al. 2003; Knigge et al. 2008; Turner & Miller 2009; Allen et al. 2011). The simplest explanation for the incidence of BAL quasars (BALQSOs) is in terms of an accretion disc wind (ADW). Within the ADW paradigm, a biconical wind rises from the accretion disc and the BALQSO fraction is associated with the covering factor of the outflow. The wind is expected to be roughly equatorial from polarisation results (Goodrich & Miller 1995; Cohen et al. 1995). ADWs offer a natural explanation for the diverse phenemonology of luminous AGN and QSOs (e.g. Murray et al. 1995; Elvis 2000). Depending on viewing angle, an observer may see a BALQSO or normal 'Type 1' quasar. Within this framework, the broad-line region (BLR) can correspond either to the dense wind base or dense clumps embedded in the outflows. Indeed, Elitzur et al. (2014) found that a disc-wind BLR scenario naturally explains the emission line evolution of AGN. A biconical wind model can also readily explain the various sub-classifications of BALQSOs: HiBALQSOs, which only exhibit higher ionization line absorption; LoBALQSOs which also show absorption in lower ionization state species such as Mg II and Al III; and FeLoBALQSOs which show further absorption in Fe II and III. In unified models, this is generally attributed to ionization stratification of the outflow (e.g. Elvis 2000).

As well as imprinting clear line absorption and emission features, disc winds may also have a profound effect on the structure and emergent *continuum* of the accretion disc itself. Mass-loss will alter the accretion rate and resultant temperature of the accretion disc, possibly explaining some of the features typically seen in luminous AGN (Knigge 1999; Laor & Davis 2014). There have been numerous difficulties when confronting theoretical accretion disc models with observations (see e.g. Blaes 1998). However, AGN spectral energy distributions (SEDs) can now, in general, be fitted well with accretion disc models when the effects of general relativity (GR), Comptonisation and mass-loss are included (Capellupo et al. 2015). Mass-loss therefore appears to be critical if an accretion disc model is to successfully fit AGN SEDs, particular in the UV region of the spectrum.

Despite the clear importance of ADWs in understanding AGN SEDs and accretion physics, much of the underlying outflow physics remains highly uncertain. Several possible driving mechanisms for ADWs have been proposed, including thermal pressure (Weymann et al. 1982; Begelman et al. 1991), magnetocentrifugal forces (Blandford & Payne 1982; Pelletier & Pudritz 1992) and radiation pressure on spectral lines ('line-driving'; Lucy & Solomon 1970; Shlosman et al. 1985; Murray et al. 1995). Of these, line-driving is possibly the most attractive, as strong absorption lines are already seen in BALQSOs and the X-ray spectra of AGN (Reeves et al. 2003; Pounds & Reeves 2009; Tombesi et al. 2010). The presence of line-locked features (Bowler et al. 2014) and the 'ghost of Ly α' (Arav et al. 1996; Arav 1996; North 2006; but see also Cottis et al. 2010) in the spectra of some BALQSOs also gives clearer evidence that line-driving is at least partially contributing to the acceleration of the wind.

The efficiency of line-driving is crucially dependent on the ionization state of the outflowing plasma, meaning that it is difficult to prevent the wind becoming over-ionized and 'failing' in the presence of strong X-rays. Murray et al. (1995) proposed a potential solution: a region of 'hitchhiking gas' that could shield the wind from the central X-ray source. Hydrodynamic simulations of line-driven disc winds also found a shielding region was required to maintain the correct ionization state (Proga et al. 2000; Proga & Kallman 2004). However, Higginbottom et al. (2014) showed that including multiple scattering means the ionizing radiation field could still reach the previously shielded regions in those particular models. An additional or alternative solution is that the wind is clumped (e.g. Hamann et al. 2013) possibly on multiple scale lengths. Local density enhancements could lower the ionization parameter of the plasma while still maintaining the same mass-loss rate and column density.

Evidence for dense substructures in AGN winds is widespread. BALQSOs show complex absorption line profiles (Ganguly et al. 2006; Simon & Hamann 2010) and exhibit variability in these profile shapes (Capellupo et al. 2011, 2012, 2014). AGN generally show variability in X-ray absorption components (e.g. Risaliti et al. 2002) and many models for the BLR consist of clumps embedded in an outflow (Krolik et al. 1981; Emmering et al. 1992; de Kool & Begelman 1995; Cassidy & Raine 1996). Clumping can be caused by magnetic confinement de Kool & Begelman (1995), or the instabilities inherent to line-driven winds (Lucy & Solomon 1970; MacGregor et al. 1979; Carlberg 1980; Owocki & Rybicki 1984, 1985). Additionally, clumping is required to explain the electron scattering wings of emission lines formed in line-driven hot star winds (Hillier 1991). Complex substructures on a variety of scales are also produced in simulations of line-driven outflows in AGN (Proga et al. 2000; Proga & Kallman 2004; Proga & Kurosawa 2010; Proga et al. 2014). Clumpy winds therefore offer an observationally motivated and theoretically predicted way to lower the ionization state of a plasma, possibly in tandem with a shielding scenario.

There has been some success using simple kinematic prescriptions for biconical disc winds to model AGN and quasar outflows (Sim et al. 2008, 2010; Higginbottom et al. 2013, hereafter H13). H13 successfully produced a benchmark model for BALQSOs. However, the model had two key drawbacks. First, an unrealistically low X-ray luminosity was required in order to prevent over-

ionization of the outflow. Second, the model failed to produce the strong emission lines required at low inclinations in a unified model. In this paper, we attempt to address these issues, and test the disc wind unification model using Monte Carlo radiative transfer (MCRT) and photoionization calculations. The paper is organised as follows. In section 2, we describe some of the important photoionization and MCRT aspects of the code. In section 3, we outline the model, including a description of our clumping implementation. In section 4, we present the results from a clumped model. In section 5 we discuss our results, focussing particular on the anisotropy of disc emission and GR effects, and finally, in section 6, we summarise our findings.

2. Ionization and Radiative Transfer

We use the MCRT code Python to carry out our radiative transfer and photoionization calculations in non-local thermodynamic equilibrium (non-LTE). The code has been used to model accreting white dwarfs (Long & Knigge 2002, hereafter LK02; Noebauer et al. 2010; Matthews et al. 2015, hereafter M15), young-stellar objects (Sim et al. 2005) and quasars (H13). These studies contain extensive detail on the code, so we only briefly describe the key elements of the global ionization calculation and other important aspects.

2.1. Line transfer

To treat line transfer, we adopt the same hybrid scheme described by M15, in which the energy flows through the system are described in terms of indivisible energy quanta of radiant or kinetic energy ('$r-$packets' and '$k-$packets' respectively; see also section 2.3). These energy packets interact with either two-level 'simple ions' or full 'macro-atoms'. The macro-atom implementation is described in full by Lucy (2002, 2003). Our scheme allows one to treat non-LTE line transfer in radiative equilibrium without approximation for elements which are identified as full macro-atoms, while maintaining the fast 'two-level' treatment of resonance lines when elements are identified as simple-ions (see M15). In this study, only H & He are treated as macro-atoms, because we expect recombination to be important in determining their level populations and resultant line emission.

2.2. Ionization Scheme

Macro-atoms have their ion and level populations derived from MC rate estimators as described by M15. Previously (LK02, H13, M15), we adopted a modified Saha approach to calculate the ionization fractions of simple-ions. We have now improved our code to explicitly solve the rate equations between ions in non-LTE. This dispenses with a number of small assumptions made in the modified Saha approach, is more numerically stable, and, in principle, allows the direct addition of extra physical processes such as Auger ionization.

We model the SED in a cell using the technique described by H13. In this scheme, the mean intensity in a series of n bands is modeled as a normalised power law in frequency ν

$$J_{\nu,i} = K_{pl}\nu^{\alpha_{pl}}, \tag{1}$$

for a band i, or an exponential

$$J_{\nu,i} = K_{exp}e^{(-h\nu/kT_{exp})}. \tag{2}$$

Here, K_{exp}, K_{pl}, T_{exp} and α_{pl} are spectral fit parameters deduced from the band-limited radiation field estimators. The ionization rate out of ion j can then be written as

$$R_{j,j+1}(J) = n_i \left(C_j n_e + \sum_{band}^{n} \int_{\nu_i}^{\nu_i+1} J_{\nu,i}\sigma_j(\nu)\nu^{-1}d\nu \right), \tag{3}$$

where σ_j is the photoionization cross-section and C_j represents the collisional ionization coefficient. The recombination rate *into* ion j is given by

$$R_{j+1,j}(T_e) = (\alpha^j_{RR} + \alpha^j_{DR} + \alpha^j_{CR})n_{j+1}n_e, \tag{4}$$

where each α^j here is the recombination rate coefficient into the ground state of ion j. The subscripts denote radiative, dielectronic and collisional (three-body) recombination, respectively. We neglect recombination to and from excited states in the simple-ion calculation. For simple-ions, we use a dilute Boltzmann equation to calculate the population of level k in ionic stage j,

$$\frac{n_{jk}}{n_j} = \frac{Wg_k}{z_j(T_R)} \exp(-E_k/kT_R). \tag{5}$$

Here z_j is the partition function of ionic stage j, T_R is the effective radiation temperature, E_k is the energy difference between level k and the ground state, and g_k is the statistical weight of level k.

2.3. Physical Processes

We include all free-free, bound-free and bound-bound heating and cooling processes in the model. For radiative transfer purposes we treat electron scattering in the Thomson limit, but take full account of Compton heating and cooling when calculating the thermal balance of the plasma (see H13). Adiabatic cooling is included and represents the only departure from strict radiative equilibrium, but is insignificant in most of the outflow.

2.4. Atomic Data

We use the same atomic data as described by LK02 and since updated by H13 and M15, with the addition of direct ionization data from Dere (2007). Photoionization cross-sections are from

TOPBASE (Cunto et al. 1993) and Verner et al. (1996). Dielectronic and radiative recombination rate coefficients are taken from the CHIANTI database version 7.0 (Dere et al. 1997; Landi et al. 2012). We use ground state recombination rates from Badnell (2006) where available, and otherwise default to calculating recombination rates from the Milne relation. Free-free Gaunt factors are from Sutherland (1998).

3. A Clumpy Biconical Disk Wind Model for Quasars

Our kinematic prescription for a biconical disc wind model follows Shlosman & Vitello (1993), and is described further by LK02, H13 and M15. A schematic is shown in figure 1, with key aspects marked. The general biconical geometry is similar to that invoked by Murray et al. (1995) and Elvis (2000) in order to explain the phenomenonology of quasars and BALQSOs.

3.1. Photon Sources

The accretion disc in our model is geometrically thin, but optically thick. We thus treat the disc as an ensemble of blackbodies with a Shakura & Sunyaev (1973) effective temperature profile. The emergent SED is then determined by the specified accretion rate ($\dot{m}$) and central BH mass (M_{BH}). All photon sources in our model are assumed to beopaque, meaning that photons which strike them are destroyed. The inner radius of the disc extends to the innermost stable circular orbit (ISCO) of the BH. We assume a Schwarzchild BH with an ISCO at 6 r_G, where $r_G = GM_{BH}/c^2$ is the gravitational radius. For a 10^9 $M_\odot$ black hole, this is equal to 8.8×10^{14} cm or $\sim 10^{-4}$ pc.

The X-ray source in our model is treated as an isotropic sphere at the ISCO, which emits r-packets according to a power law in flux with index α_X, of the form

$$F_X(\nu) = K\nu^{\alpha_X}. \tag{6}$$

The normalisation, K_X of this power law is such that it produces the specified 2-10 keV luminosity, L_X. In addition to the disc and X-ray source, the wind is able to reprocess radiation. However, new photon packets are not produced in the wind (as in LK02). Instead, this reprocessing is dealt with by enforcing strict radiative equilibrium (*modulo* adiabatic cooling; see section 2.3) via an indivisible energy packet constraint (see Lucy 2002, M15).

3.2. Kinematics and Geometry

In our model, a biconical disc wind rises from the accretion disc between launch radii r_{min} and r_{max}. The opening angles of the wind are set to θ_{min} and θ_{max}. The poloidal velocity along each

individual streamline at a poloidal distance l is then given by

$$v_l = v_0 + [v_\infty(r_0) - v_0] \frac{(l/R_v)^\alpha}{(l/R_v)^\alpha + 1}, \tag{7}$$

where v_0 is the velocity at the base of the streamline, α is an exponent governing how quickly the wind accelerations and R_v is the 'acceleration length', defined as the distance at which the outflow reaches half of its terminal velocity, v_∞. The terminal velocity is set to a fixed multiple of the escape velocity, v_{esc}, at the base of the streamline (radius r_0). The rotational velocity, v_ϕ, is initially Keplerian ($v_k = [GM/r_0]^{1/2}$), and the wind conserves specific angular momentum, such that

$$v_\phi r = v_k r_0. \tag{8}$$

The velocity law is crucial in determining the output spectra, as it affects not only the projected velocities along the line of sight, but also the density and ionization state of the outflow. A wind which accelerates more slowly will have a denser wind base with correspondingly different ionization and emission characteristics.

3.3. Clumping

To allow for clumping in our outflow we adopt a simple approximation used extensively in stellar wind modelling, known as *microclumping* (Hamann & Koesterke 1998). The key assumption here is that typical clump sizes are much smaller than the typical photon mean free path, and thus the clumps are both geometrically and optically thin. This approach allows one to introduce a 'filling factor', f, which is the fraction of the volume of the plasma filled by clumps. The intra-clump medium is assumed to be a vacuum. We can then introduce the density enhancement, D, which is defined as

$$D = \frac{1}{f}. \tag{9}$$

We then multiply all densities in the model by D, and all emitting volumes by f. This has the effect of enhancing all emissivities and opacities that scale with the square of density (such as collisional excitation and recombination) by a factor D. All processes that scale linearly with density (such as electron scattering and bound-free opacity) will remain unchanged for a given ionization state.

Clumping the wind has an important effect on the ionization state and has been proposed as a solution to the so-called 'over-ionization problem' in disc winds (REFs). This is the main motivation for incorporating microclumping into our model. This treatment is first-order; it does not adequately represent the complex substructures and stratifications in ionization state we expect in AGN outflows. Nevertheless, clumping is clearly important in these flows, and this parameterization allows a simple estimate for the effect clumping might have on the ionization state and emergent line emission. It is also encouraging that microclumping has been used successfully in fits to O-star wind spectra (Hillier 1991).

4. Results and Discussion

Here we describe the results from our model, the parameters of which are shown in table 1. Parameters differing from the benchmark model of H13 are highlighted with an asterisk. This set of parameters was arrived at by conducting a limited grid search over a 5-dimensional parameter space involving the variables r_{min}, θ_{min}, f, α and R_V. The full grid, including output spectral files and plots can be found at `jhmatthews.github.io/quasar-wind-grid/`. We evaluated these models qualitatively based on the following criteria:

- Does the model maintain the right ionization state to produce strong BALs?
- Does significant line emission emerge at low inclinations?
- Do H recombination lines appear in the spectrum?
- Do a certain range of angles produce LoBAL features?
- Does the model compare favourably to quasar composite spectra?

In this section, we present one of the most promising models and discuss the various successes and failures. This allows us to gain insight into fundamental geometrical and physical constraints and assess the potential for unification.

4.1. Physical Conditions and Ionization State

Figure 2 shows the physical properties of the wind. The wind rises slowly from the disc at first, with clumped densities of $n_H \sim 10^{11}$ cm^{-3} close to the disc plane. The flow then accelerates over a scale length of $R_V = 10^{19}$ cm up to a terminal velocity equal to the escape velocity at the streamline base ($\sim 10,000$ km s^{-1}). This gradual acceleration means that the wind exhibits a stratified ionization structure, with low ionization material in the base of the wind giving way to highly ionized plasma further out. By clumping the wind, we are able to produce the range of ionization states observed in quasars and BALQSOs, while adopting a realistic $2-10$ keV X-ray luminosity of $L_X = 10^{45}$ ergs s^{-1}. Without clumping, this wind would be over-ionized to the extent that opacities in e.g., C IV would be entirely negligible (see H13).

One common way to quantify the ionization state of a plasma is through the ionization parameter, U_H, given by

$$U_H = \frac{4\pi}{n_H c} \int_{13.6\mathrm{eV}}^{\infty} \frac{J_\nu d\nu}{h\nu}. \tag{10}$$

where n_H is the local number density of H, and ν denotes photon frequency. Shown in figure 2, the ionization parameter is a useful measure of the global ionization state, as it represents the ratio of the number density of H ionizing photons to the local H density. It is, however, a poor

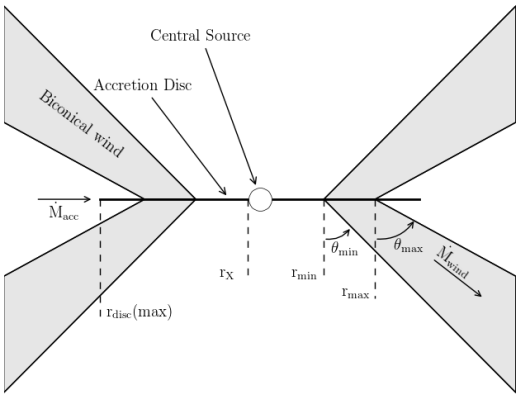

Fig. 1.— A cartoon showing the geometry and some key parameters of our biconical wind model.

Free Parameters	Value
M_{BH}	1×10^9 M$_\odot$
$\dot{M}_{acc}$	5 $M_\odot yr^{-1} \simeq 0.2$ $\dot{M}_{Edd}$
α_X	-0.9
L_X	10^{45} ergs s^{-1}*
$r_{disc}(min) = r_X$	$6r_g = 8.8 \times 10^{14}$ cm
$r_{disc}(max)$	$3400r_g = 5 \times 10^{17}$ cm
$\dot{M}_{wind}$	5 $M_\odot yr^{-1}$
r_{min}	$300r_g = 4.4 \times 10^{16}$ cm
r_{max}	$600r_g = 8.8 \times 10^{16}$ cm
θ_{min}	70.0°
θ_{max}	82.0°
λ	0
$v_\infty(r_0)$	$v_{esc}(r_0)$
R_v	10^{19}cm*
α	0.6*
f	0.01*

Table 1: Wind geometry parameters used in the model.

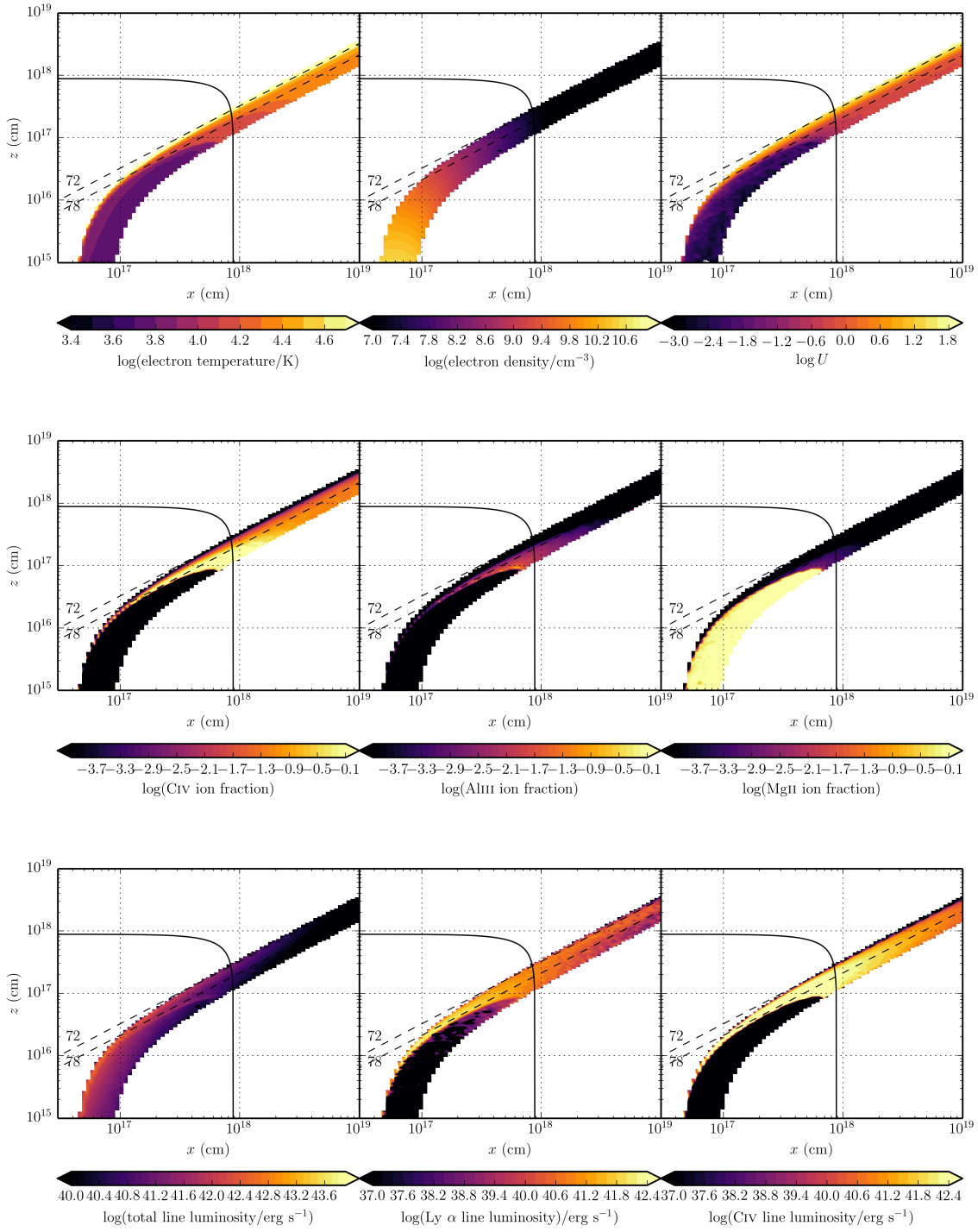

Fig. 2.— Physical properties of the outflow, shown by the coloured contours. The solid black line marks a sphere at 1000 r_G. The dotted lines show the 72° and 78° sightlines to the centre of the system, and illustrate that different sightlines intersect material of different ionization states.

representation of the ionization state of species such as C IV as it encodes no information about the shape of the SED. In our case, the X-ray photons are dominant in the photoionization of the UV resonance line ions. This explains why a factor of 100 increase in X-ray luminosity requires a clumping factor of 0.01, even though the value of U_H decreases by only a factor of ~ 10 compared to H13. This is also the reason for significant Lyman edge photoabsorption at the highest inclinations (see section 4.3).

Clumping also causes the total line luminosity to increase dramatically, as recombination and collisional excitation are both proportional to n_e^2. This line emission typically emerges on the edge of the wind nearest the central source. The location of the line emitting regions is dependent on the ionization state, as well as the X-rays heating the plasma. The radii of these emitting regions is important, and can be compared to observations. As shown in figure 2, the C IV line in our model is typically formed between $100 - 1000\ r_G$ ($\sim 10^{17} - 10^{18}$ cm). This is in rough agreement with the reverberation mapping results of Kaspi (2000) for the $2.6 \times 10^9 M_\odot$ quasar S5 0836+71, and also compares favourably with microlensing measurements of the size of the C IV emission line region in the BALQSO H1413+117 (O'Dowd et al. 2015).

4.2. Synthetic Spectra

Figure 3 shows the synthetic spectrum in the UV from our model. We also show a comparison to composite quasar and BALQSO spectra. We show a cartoon illustrating how geometric effects determine the output spectra in figure 4.

4.2.1. Broad absorption lines

The UV spectrum is characterised by strong BAL profiles at high inclinations ($> 70°$). This highlights the first success of our model: clumping means the correct ionization state is maintained in the presence of strong X-rays, allowing large resonance line opacities. At the highest inclinations, the cooler, lower ionization material at the base of the wind starts to intersect the line of sight. This produces multiple absorption lines in lower ionization species such as Mg II, Al III and Fe II. The potential links to LoBALQSOs and FeLoBALQSOs are discussed in section 2.4.

The high ionization BAL profiles are often saturated, and the location in velocity space of the strongest absorption in the profile varies with inclination. At lower inclinations, the strongest absorption occurs at the red edge, whereas at high inclinations (and for the strongest BALs) the trough has a sharp edge at the terminal velocity. This offers one potential explanation for the wide range of BALQSO absorption line shapes (see e.g. Trump et al. 2006; Knigge et al 2008). In addition, the line profile shape is strongly dependent on the density, ionization and velocity profiles intersected by the line of sight. Thus, small tweaks of the velocity law and angular distributions of streamlines can dramatically alter the shape of the line.

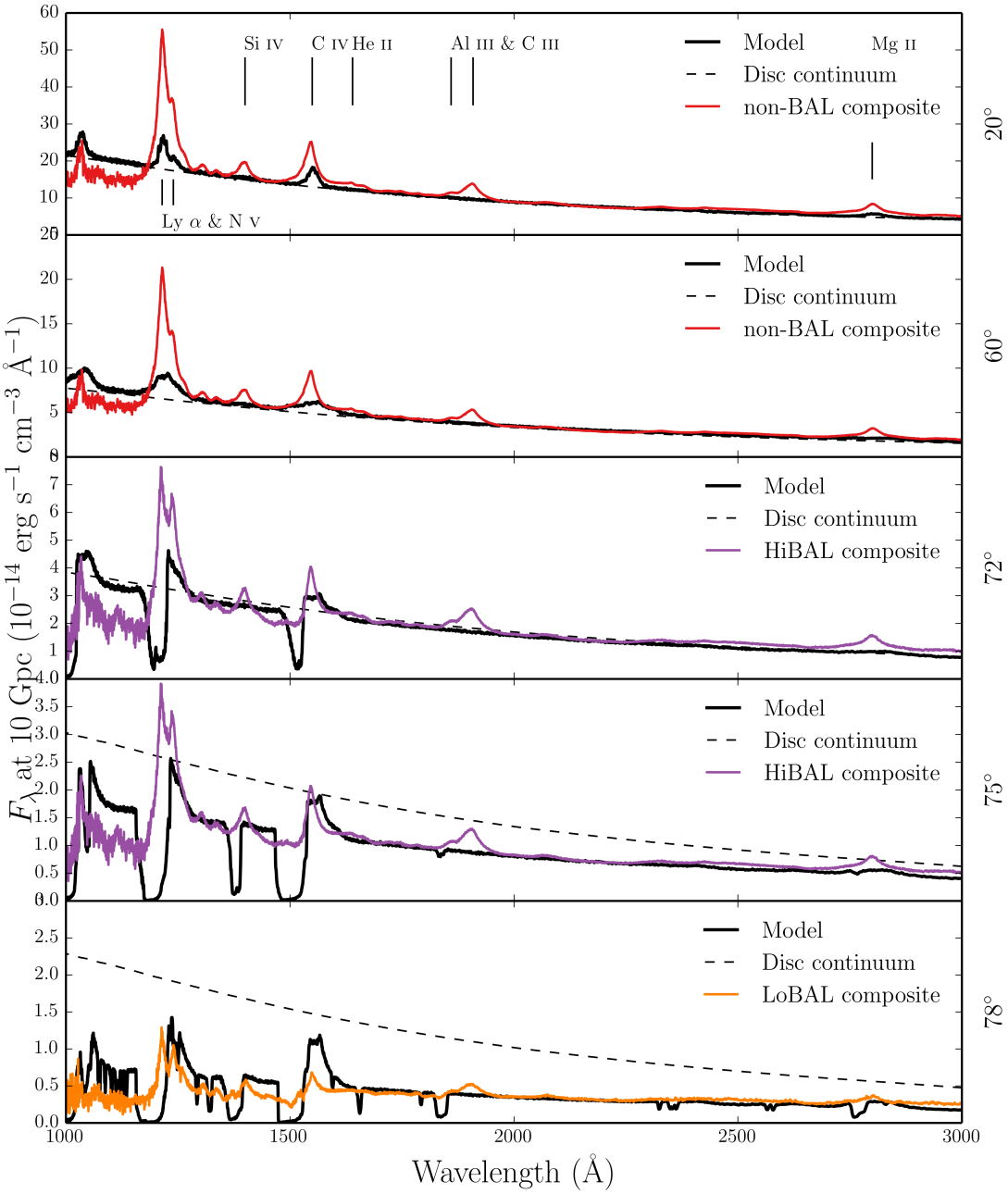

Fig. 3.— Synthetic spectra at five viewing angles in our. The coloured lines show different quasar and BAL quasar composites, and the dotted line shows a disc only continuum to show the effect of the outflow on the continuum level.

Nonblack saturation is observed in the absorption troughs of BALQSOs (Arav et al. 1999b,a). This can be caused either by partial covering of the continuum source or by scattered contributions to the BAL troughs, necessarily from an opacity source not cospatial with the BAL forming region. The scattered light explanation is supported by spectropolarimetry results (Lamy & Hutsemékers 2000). Our spectra do not show nonblack saturation. Instead, we find black, saturated troughs at angles $i > 73°$, and the BALs are non-saturated at lower inclinations. The reasons for this are readily apparent. First, the microclumping assumption does not allow for porosity in the wind, meaning that it does not naturally produce a partial covering absorber. To do this, an alternative approach such as *macroclumping* would be required (e.g. Šurlan et al. 2012; Hamann et al. 2008). Second, our wind does not have a significant scattering contribution along sightlines which do not pass through the BAL region, meaning that any scattered contribution is obscured by the saturated troughs. This suggests that either the scattering cross-section of the wind must be increased (with higher mass loss rates or covering factors), or that an additional source of electron opacity is required, potentially in a polar direction above the disc.

4.2.2. Broad emission lines

We find that the model can produce significant line emission at low inclinations, particular in C IV, and the improved treatment of recombination results in a strong Ly α line. In the context of unification, this is a promising result, and shows that a biconical wind can produce significant emission at 'quasar-like' angles. To assess the ability of the model to match real quasar spectra, we also show *Sloan Digital Sky Survey* (SDSS) quasar composites from Reichard et al. (2003), normalised to the flux at 2000Å in each panel. We do not produce the semi-forbidden intercombination lines seen in quasar spectra because we currently do not have a treatment for semi-forbidden lines. This is especially noticable with the strong C III] 1909Å line in the quasar composite spectra. The critical density of the C III] 1909Å line is $n_e \sim 10^{9.5}$ cm^{-3}, which is higher than much of the outer portion of our wind. We therefore expect intercombination lines to become

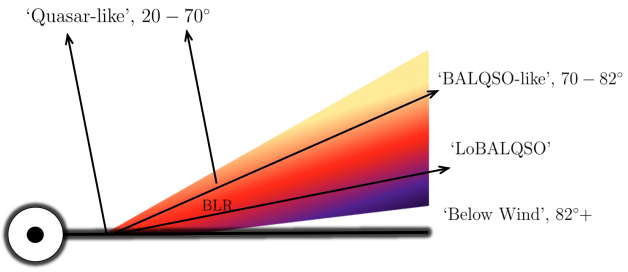

Fig. 4.— A cartoon describing the broad classes of sightline in our model, illustrates how geometric effects lead to the different emergent spectra. The colour gradient is approximate, but indicates the stratified ionization structure, from highly ionized (yellow) to low ionization (purple) material.

important coolants in the outer portion of the wind.

The model produces strong emission lines in C IV, N V and Ly α, as well as a weak Mg II line. The shapes and widths of these lines match the composites fairly well. However, the line-to-continuum ratios at low inclinations in our model are significantly weaker than the quasar composites. Increasing the density of the outflow, by altering the mass loss rate or velocity law, can produce more line emission. However, the red wing of the BAL profiles is generally stronger than seen in BALQSO spectra and composites. This illustrates a fundamental problem with a geometric unification model such as this: that the line-to-continuum ratios at low inclinations are significantly affected by disc foreshortening and limb darkening. The angular distribution of the disc radiation is clearly crucially important in determining the emergent line ratios.

4.2.3. The Disc SED

When comparing BALQSO and quasar composites, it is apparent that they possess remarkably similar line strengths and widths (e.g. Reichard et al. 2003). This presents a challenge to our model, as well as the geometric unification picture in general. Limb darkening and foreshortening causes the disc continuum emission to be strongly anisotropic, yet the line emission in our models is much more isotropic. This has the effect of enhancing the line-to-continuum ratios at high inclinations. To construct a scenario where emission line equivalent widths are comparable at all inclinations requires significant fine-tuning when considering a classical thin disc. An alternative, simpler solution is that the emergent continuum is roughly isotropic.

General relativistic effects – specifically, light bending and relativistic beaming – can cause the accretion disc SED to become more isotropic (e.g. Zhang et al. 1997; Muñoz-Darias et al. 2013). To generate GR disc spectra, we use the code AGNSPEC (Hubeny et al. 2000; Davis & Hubeny 2006; Davis et al. 2007). The output flux at three different wavelengths as a function of inclination for an AGNSPEC model with the same disc and BH parameters as our clumpy wind model is shown in figure 5. The effects of GR on an AGN disc are much less extreme in the UV portion of the spectrum than the calculations by Zhang et al. (1997) for the X-rays in X-ray binaries. As a result, the disc emission is still strongly anisotropic. GR alone therefore cannot explain the line ratio trends in quasars by making the disc emit more isotropically. This supports the findings of Risaliti et al. (2011), who find that EW distributions in quasars are consistent with anisotropic emission from optically thick, disc-like structures for *both* the continuum source and BLR. We will explore these ideas further in a future study.

4.3. X-ray Properties and Broadband SEDs

Figure 6 shows the emergent monochromatic luminosity (L_ν) at 2 keV and plotted against L_ν at 2500Å for a number of different viewing angles in our model. The monochromatic luminosities

are calculated from the synthetic spectra and thus include the effects of wind reprocessing and attenuation. In addition to model outputs, we also show the BALQSO sample of Saez et al. (2012) and luminous AGN and quasar samples from Steffen et al. (2006). The best fit relation from Steffen et al. (2006) is also shown. For low inclination, 'quasar-like' viewing angles, we now show excellent agreement with AGN samples. The gradient from 20° to 60° in our models is caused by a combination of disc foreshortening/limb-darkening (resulting in a lower L_{2500} for higher inclinations) and the fact that the disk is opaque, and thus the X-ray source subtends a smaller solid angle at high inclinations (resulting in a lower L_{2keV} for higher inclinations).

The low inclination, 'BALQSO-like' viewing angles show moderate agreement with the data, and are X-ray weak due to bound-free and electron scattering opacities in the wind. Typically, BALQSOs show strong X-ray absorption with columns of $N_H \sim 10^{23}$ cm^{-2} (Green & Mathur 1996; Mathur et al. 2000; Green et al. 2001; Grupe et al. 2003). This is often cited as evidence that the BAL outflow is shielded from the X-ray source, especially as sources with strong X-ray absorption tend to exhibit deep BAL troughs and high outflow velocities (Brandt et al. 2000; Laor & Brandt 2002; Gallagher et al. 2006). Our results imply that the clumpy BAL outflow itself can be responsible for the strong X-ray absorption, and supports Hamann et al.'s (2013) suggestion that this explains the weaker X-ray absorption in mini-BALs compared to BALQSOs.

Our models slightly over-predict the emergent X-ray luminosity at BAL angles, although we are limited by poor sample sizes. If BALQSOs were *intrinsically* X-ray weak (as suggested by, e.g. Morabito et al. 2013), our isotropic assumption foe the X-ray source would be incorrect. A polar-biased X-ray source would result in a lower clumping factor being required in our model. Our specific wind prescription will also affect the opacities, densities and resultant ionization structure, which can change the absorption characteristics and resultant luminosities. Nevertheless, our input X-ray spectrum now reproduces the X-ray properties of a luminous quasar as an output, and at least some BAL angles match the observations. This satisifies the first-order requirement for the X-ray properties of a unified quasar model.

4.4. LoBALs and ionization stratification

At certain sightlines, our model now produces blue-shifted BALs in Al III and Mg II– the absorption lines seen in LoBALQSOs, and we even see absorption in Fe II at the highest inclinations. Line profiles in velocity space for C IV, Al III and Mg II, are shown in figure 7 for a range of BALQSO viewing angles. We find that ionization stratification of the wind causes lower ionization material has a smaller covering factor, as demonstrated by figures 2 and 7. This confirms the behaviour expected from a unification model such as Elvis (2000). LoBALs are only present at viewing angles close to edge-on ($i > 75°$), as predicted by polarisation results (Brotherton et al. 1997). There is also a correlation between the strength of LoBAL features and the amount of continuum attenuation at that sightline, particularly blueward of the Lyman edge as the low ionization base intersects the line-of-sight. Our model therefore predicts that LoBALQSOs and FeLoBALQSOs have stronger

Lyman edge absorption and be more Compton-thick than HiBALQSOs and Type 1 quasars. An edge-on scenario also offers a potential explanation for the rarity of LoBAL and FeLoBAL quasars, due to a foreshortened and attenuated continuum, although, as noted in section 4.2.3, BAL fraction inferences are fraught with complex selection effects.

5. Summary

We have carried out MCRT simulations using a simple prescription for a biconical disc wind, with the aim of expanding on the work of H13 and assessing the viability of such a model for geometric unification of quasars. We find the following main points:

1. We have introduced a first-order treatment of clumping in our model, and found that it can now maintain the required ionization state while agreeing well with the X-ray properties of AGN/QSOs.

2. We have shown that the degree of ionization stratification in the model is sufficient that LoBAL line profiles are seen at a subset of viewing angles, and Fe II absorption is seen at particularly high inclinations.

3. We find that clumping also causes a significant increase in the strength of the emission lines produced by the model. This is true both of collisionally excited resonance lines (such as C IV, N V) and recombination lines (such as Ly α, H α and the Balmer series).

4. The line EWs in our models increase with inclination. BAL and non-BAL quasar composites have comparable EWs, so our model fails to reproduce this behaviour. This is due to a fundamental constraint discussed further in section 5. If the BLR emits fairly isotropically then for a foreshortened, limb-darkened classical thin accretion disc it is simply not possible to achieve line ratios at low inclinations that are comparable to those at high inclinations. This is a robust conclusion which is independent of the assumed BLR geometry and size.

5. We have examined the effect of GR on our disc SED, using the disc atmosphere and GR ray-tracing code AGNSPEC. While including GR effects does cause the disc SED to become slightly more isotropic, the effect is not large enough to produce uniform line to continuum ratios with viewing angle. We briefly discuss other solutions.

Our work confirms a number of expected outcomes from a geometric unification model, and suggests that a simple biconical geometry such as this can come close to explaining much of the phenomenology of quasars. Nevertheless, our conclusions pose a clear challenge to the current disc wind unification picture.

Acknowledgements

The work of JHM, SWM, NSH and CK is supported by the Science and Technology Facilities Council (STFC), via two studentships and a consolidated grant, respectively. We would like to thank Omer Blaes, Ivan Hubeny and Shane Davis for their assistance with AGNSPEC. We would also like to thank Daniel Proga, Daniel Capellupo, Sam Connolly and Dirk Grupe for useful discussions. Simulations were conducted using PYTHON version 79c, and made use of the IRIDIS High Performance Computing Facility at the University of Southampton. Figures were produced using `matplotlib` (Hunter 2007).

REFERENCES

Allen J. T., Hewett P. C., Maddox N., Richards G. T., Belokurov V., 2011, MNRAS 410, 860

Arav N., 1996, ApJ 465, 617

Arav N., Becker R. H., Laurent-Muehleisen S. A., Gregg M. D., White R. L., Brotherton M. S., de Kool M., 1999a, ApJ 524, 566

Arav N., Korista K. T., Barlow T. A., Begelman, 1995, Nature 376, 576

Arav N., Korista K. T., de Kool M., Junkkarinen V. T., Begelman M. C., 1999b, ApJ 516, 27

Badnell N. R., 2006, ApJs 167, 334

Begelman M., de Kool M., Sikora M., 1991, ApJ 382, 416

Blaes O., 1998, in S. S. Holt, T. R. Kallman (eds.), American Institute of Physics Conference Series, Vol. 431 of *American Institute of Physics Conference Series*, p. 161

Blandford R. D., Payne D. G., 1982, MNRAS 199, 883

Bowler R. A. A., Hewett P. C., Allen J. T., Ferland G. J., 2014, MNRAS 445, 359

Brandt W. N., Laor A., Wills B. J., 2000, ApJ 528, 637

Brotherton M. S., Tran H. D., van Breugel W., Dey A., Antonucci R., 1997, ApJ Letters 487, L113

Capellupo D. M., Hamann F., Barlow T. A., 2014, MNRAS 444, 1893

Capellupo D. M., Hamann F., Shields J. C., Rodríguez Hidalgo P., Barlow T. A., 2011, MNRAS 413, 908

Capellupo D. M., Hamann F., Shields J. C., Rodríguez Hidalgo P., Barlow T. A., 2012, MNRAS 422, 3249

Capellupo D. M., Netzer H., Lira P., Trakhtenbrot B., Mejía-Restrepo J., 2015, MNRAS 446, 3427

Carlberg R. G., 1980, ApJ 241, 1131

Cassidy I., Raine D. J., 1996, A&A 310, 49

Cohen M. H., Ogle P. M., Tran H. D., Vermeulen R. C., Miller J. S., Goodrich R. W., Martel A. R., 1995, ApJ Letters 448, L77

Cottis C. E., Goad M. R., Knigge C., Scaringi S., 2010, MNRAS 406, 2094

Cunto W., Mendoza C., Ochsenbein F., Zeippen C. J., 1993, A&A 275, L5

Davis S. W., Hubeny I., 2006, ApJs 164, 530

Davis S. W., Woo J.-H., Blaes O. M., 2007, ApJ 668, 682

de Kool M., Begelman M. C., 1995, ApJ 455, 448

Dere K. P., 2007, A&A 466, 771

Dere K. P., Landi E., Mason H. E., Monsignori Fossi B. C., Young P. R., 1997, A&As 125, 149

Elitzur M., Ho L. C., Trump J. R., 2014, MNRAS 438, 3340

Elvis M., 2000, ApJ 545, 63

Emmering R. T., Blandford R. D., Shlosman I., 1992, ApJ 385, 460

Fabian A. C., 2012, ARAA 50, 455

Gallagher S. C., Brandt W. N., Chartas G., Priddey R., Garmire G. P., Sambruna R. M., 2006, ApJ 644, 709

Ganguly R., Brotherton M. S., 2008, ApJ 672, 102

Ganguly R., Sembach K. R., Tripp T. M., Savage B. D., Wakker B. P., 2006, ApJ 645, 868

Goodrich R. W., Miller J. S., 1995, ApJ Letters 448, L73

Green P. J., Aldcroft T. L., Mathur S., Wilkes B. J., Elvis M., 2001, ApJ 558, 109

Green P. J., Mathur S., 1996, ApJ 462, 637

Grupe D., Mathur S., Elvis M., 2003, AJ 126, 1159

Hamann F., Chartas G., McGraw S., Rodriguez Hidalgo P., Shields J., Capellupo D., Charlton J., Eracleous M., 2013, MNRAS 435, 133

Hamann W.-R., Koesterke L., 1998, A&A 335, 1003

Hamann W.-R., Oskinova L. M., Feldmeier A., 2008, in W.-R. Hamann, A. Feldmeier, L. M. Oskinova (eds.), Clumping in Hot-Star Winds, 75

Häring N., Rix H.-W., 2004, ApJ Letters 604, L89

Hazard C., Mackey M. B., Shimmins A. J., 1963, Nature 197, 1037

Higginbottom N., Knigge C., Long K. S., Sim S. A., Matthews J. H., 2013, MNRAS 436, 1390

Higginbottom N., Proga D., Knigge C., Long K. S., Matthews J. H., Sim S. A., 2014, ApJ 789, 19

Hillier D. J., 1991, A&A 247, 455

Hubeny I., Agol E., Blaes O., Krolik J. H., 2000, ApJ 533, 710

Hunter J. D., 2007, Computing In Science & Engineering 9(3), 90

Kellermann K. I., Sramek R., Schmidt M., Shaffer D. B., Green R., 1989, AJ 98, 1195

King A., 2003, ApJ Letters 596, L27

King A., 2005, ApJ Letters 635, L121

Knigge C., 1999, MNRAS 309, 409

Knigge C., Scaringi S., Goad M. R., Cottis C. E., 2008, MNRAS 386, 1426

Krolik J. H., McKee C. F., Tarter C. B., 1981, ApJ 249, 422

Lamy H., Hutsemékers D., 2000, A&A 356, L9

Landi E., Del Zanna G., Young P. R., Dere K. P., Mason H. E., 2012, ApJ 744, 99

Laor A., Brandt W. N., 2002, ApJ 569, 641

Laor A., Davis S. W., 2014, MNRAS 438, 3024

Long K. S., Knigge C., 2002, ApJ 579, 725

Lucy L. B., 2002, A&A 384, 725

Lucy L. B., 2003, A&A 403, 261

Lucy L. B., Solomon P. M., 1970, ApJ 159, 879

MacGregor K. B., Hartmann L., Raymond J. C., 1979, ApJ 231, 514

Marscher A. P., 2006, in P. A. Hughes, J. N. Bregman (eds.), Relativistic Jets: The Common Physics of AGN, Microquasars, and Gamma-Ray Bursts, Vol. 856 of *American Institute of Physics Conference Series*, p. 1

Mathur S., Green P. J., Arav N., Brotherton M., Crenshaw M., deKool M., Elvis M., Goodrich R. W., Hamann F., Hines D. C., Kashyap V., Korista K., Peterson B. M., Shields J. C., Shlosman I., van Breugel W., Voit M., 2000, ApJ Letters 533, L79

Matthews J. H., Knigge C., Long K. S., Sim S. A., Higginbottom N., 2015, MNRAS 450, 3331

Morabito L. K., Dai X., Leighly K. M., Sivakoff G. R., Shankar F., 2013, ArXiv e-prints

Muñoz-Darias T., Coriat M., Plant D. S., Ponti G., Fender R. P., Dunn R. J. H., 2013, MNRAS 432, 1330

Murray N., Chiang J., Grossman S. A., Voit G. M., 1995, ApJ 451, 498

Noebauer U. M., Long K. S., Sim S. A., Knigge C., 2010, ApJ 719, 1932

North M., Knigge C., Goad M., 2006, MNRAS 365, 1057

O'Dowd M. J., Bate N. F., Webster R. L., Labrie K., Rogers J., 2015, ArXiv e-prints

Owocki S. P., Rybicki G. B., 1984, ApJ 284, 337

Owocki S. P., Rybicki G. B., 1985, ApJ 299, 265

Pelletier G., Pudritz R. E., 1992, ApJ 394, 117

Perley R. A., Dreher J. W., Cowan J. J., 1984, ApJ Letters 285, L35

Potash R. I., Wardle J. F. C., 1980, ApJ 239, 42

Pounds K. A., Reeves J. N., 2009, MNRAS 397, 249

Proga D., Jiang Y.-F., Davis S. W., Stone J. M., Smith D., 2014, ApJ 780, 51

Proga D., Kallman T. R., 2004, ApJ 616, 688

Proga D., Kurosawa R., 2010, in L. Maraschi, G. Ghisellini, R. Della Ceca, F. Tavecchio (eds.), Accretion and Ejection in AGN: a Global View, Vol. 427 of *Astronomical Society of the Pacific Conference Series*, 41

Proga D., Stone J. M., Kallman T. R., 2000, ApJ 543, 686

Reeves J. N., O'Brien P. T., Ward M. J., 2003, ApJ Letters 593, L65

Reichard T. A., Richards G. T., Hall P. B., Schneider D. P., Vanden Berk D. E., Fan X., York D. G., Knapp G. R., Brinkmann J., 2003, AJ 126, 2594

Risaliti G., Elvis M., Nicastro F., 2002, ApJ 571, 234

Risaliti G., Salvati M., Marconi A., 2011, MNRAS 411, 2223

Shakura N. I., Sunyaev R. A., 1973, A&A 24, 337

Shlosman I., Vitello P., 1993, ApJ 409, 372

Shlosman I., Vitello P. A., Shaviv G., 1985, ApJ 294, 96

Silk J., Rees M. J., 1998, A&A 331, L1

Sim S. A., Drew J. E., Long K. S., 2005, MNRAS 363, 615

Sim S. A., Long K. S., Miller L., Turner T. J., 2008, MNRAS 388, 611

Sim S. A., Miller L., Long K. S., Turner T. J., Reeves J. N., 2010, MNRAS 404, 1369

Simon L. E., Hamann F., 2010, MNRAS 409, 269

Springel V., Di Matteo T., Hernquist L., 2005, ApJ Letters 620, L79

Sutherland R. S., 1998, MNRAS 300, 321

Tombesi F., Cappi M., Reeves J. N., Palumbo G. G. C., Yaqoob T., Braito V., Dadina M., 2010, A&A 521, A57

Turner T. J., Miller L., 2009, AAPR 17, 47

Šurlan B., Hamann W.-R., Kubát J., Oskinova L. M., Feldmeier A., 2012, A&A 541, A37

Verner D. A., Ferland G. J., Korista K. T., Yakovlev D. G., 1996, ApJ 465, 487

Weymann R. J., Morris S. L., Foltz C. B., Hewett P. C., 1991, ApJ 373, 23

Weymann R. J., Scott J. S., Schiano A. V. R., Christiansen W. A., 1982, ApJ 262, 497

Zhang S. N., Cui W., Chen W., 1997, ApJ Letters 482, L155

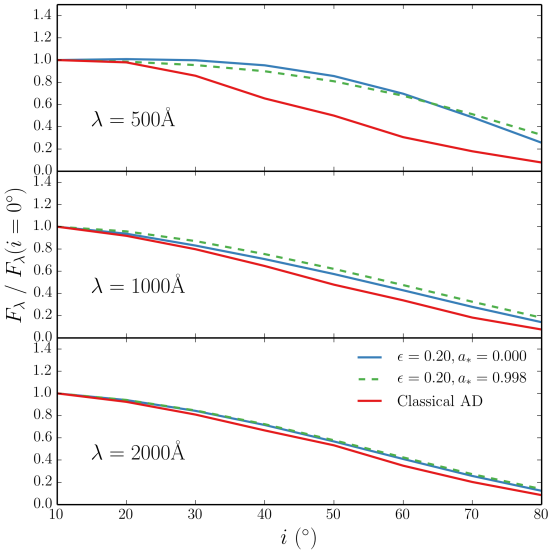

Fig. 5.— F_λ for three different wavelengths as a function of inclination from AGNSPEC models, compared to a classical AD. The AGNSPEC models are computed for Kerr and Scharzschild BHs with the same M_{BH} and $\dot{m}$ as our model.

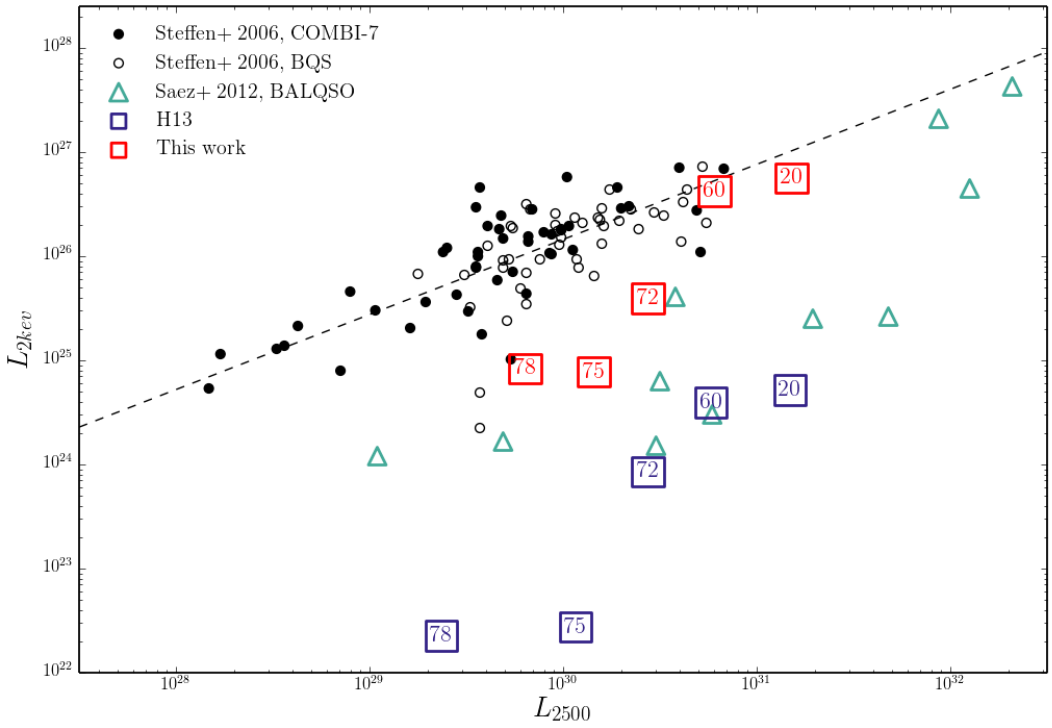

Fig. 6.— X-ray properties of the H13 (purple squares) and clumped model (red squares), plotted against monochromatic luminosity at 2500Å. The points are labeled according to inclination; angles $> 70°$ correspond to BALs in our scheme. Also plotted are the samples considered by Saez et al. 2012 on a similar plot; The COMBI-7 AGN and the BQS samples Steffen et al. (2006) and the Saez et al. (2012) sample of BALQSOs. The dotted lines show the best fit relations for non-BALQSOs from Steffen et al. (2006).

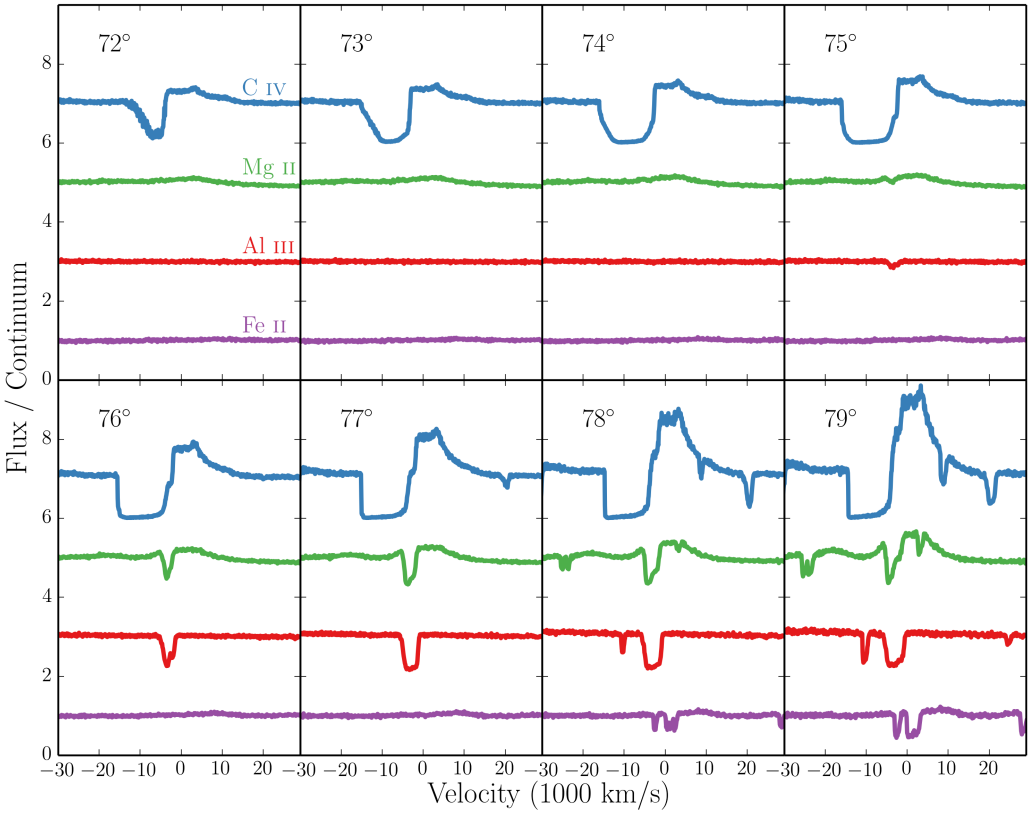

Fig. 7.— C IV, Mg II, Al III and Fe II line profiles for wind angles from $72 - 79°$. The profiles are plotted relative to the local continuum with an offset applied for clarity. Lower ionization profiles appear at a subset of high inclinations, compared to the ubiquitous C IV profile.